A Demonstration of Dual K-Band Frequency Radiometry With the Deep Space Network 70-Meter Antennas

G. Lanyi[1] and C. Naudet[1]

Brightness temperatures measured at frequencies of 19.8 and 26.3 GHz are utilized to obtain the line-of-sight water-vapor path delays that are compared with nearby Global Positioning System (GPS) and dedicated water-vapor radiometer measurements. The presented method of radiometric determination of water-vapor-induced path delays allows direct calibration of range measurements at the full range of elevation angles. The application of an a priori linear water-vapor retrieval coefficient to these exploratory measurements indicates an agreement with stochastically estimated GPS values at a level range of 0.2 to 0.8 cm at zenith. The calculated mean zenith-delay difference between these techniques is up to 0.4 cm. The known sources of these discrepancies are (1) the presence of radio sources in the measurements, (2) an inadequate brightness-temperature calibration, (3) water-vapor retrieval algorithm uncertainties, and (4) an inadequate method of GPS estimation of delays. From the current data, the lowest achievable zenith path-delay error is estimated to be 0.03 cm; that is an order of magnitude lower than the above discrepancies.

I. Introduction

Uncalibrated water-vapor-induced path delay may be a significant error in range measurements at radio frequencies. Routine determination of water-vapor path delays by radiosonde measurements is largely impractical, and meteorological surface measurements give only a crude estimate of these delays. There are two practical methods for reducing the effects of water-vapor path delay, stochastic estimation [1–4] and calibration by dedicated water-vapor radiometry [5–16,38]. The latter calibration technique is the subject of this article. The primary factors that affect the accuracy of water-vapor radiometric measurements are the absolute calibration and stability of the brightness-temperature measurements and the conversion of the brightness temperatures into water-vapor path-delay values. The stability of brightness-temperature measurements has been steadily improved during the last 30 years in dedicated water-vapor radiometers (WVRs), and the current limiting factor appears to be the error associated with conversion of brightness temperatures into water-vapor path delays. There are also secondary sources of errors that affect the water-vapor path-delay calibration of a range measurement: the distance between

[1] Tracking Systems and Applications Section.

The research described in this publication was carried out by the Jet Propulsion Laboratory, California Institute of Technology, under a contract with the National Aeronautics and Space Administration.

a dedicated WVR and the ranging antenna, the elevation-angle limits imposed by the large beam width of the past WVRs, and the mismatch between the antenna beam size of the ranging antenna and the WVR [17,18]. Clearly, using the ranging antenna as a WVR should result in the best calibration of the water-vapor path delay, but the cost and complexity caused by switching to the additional water-vapor emission (K-band) frequencies usually prevent such an application.

The Deep Space Network (DSN) of the National Aeronautics and Space Administration (NASA) employs three groups of antennas situated in Australia, California, and Spain. This network provides the communication link between the ground and certain space probes and assists the navigation of these probes by employing absolute and differential range measurements. The antennas also are utilized for a variety of radio science experiments that may require water-vapor path-delay calibration. Currently, the antennas are mostly operated at S- and X-band frequencies (2.3 and 8.4 GHz, respectively). However, DSN antennas are being equipped with K-band (19- to 26.5-GHz) and Ku-band (31.8- to 32.1-GHz) receivers. These improvements [19,20] were made to serve future communication needs and the current space-based very long baseline interferometry (VLBI) projects. In addition, the computer-based control of the receiver-system hardware, which introduced the needed flexibility for the development of new techniques, has been significantly improved. This automated receiver system offers the possibility of simultaneous use of K-band for VLBI data acquisition and for an in-beam WVR as well.

During the period between June and November of 1998, a few observing sessions of radio sources were conducted to test the performance and operation of the new K-band receiving systems. These observations involved brightness-temperature measurements of radio sources of quasars with single antennas and VLBI observation of radio sources by dual 70-m antennas at Goldstone, California, and Tidbinbilla, Australia. Promptly after the measurements were taken, it was realized that some of these measurements could serve as the foundation of an exploratory road toward direct dual-frequency water-vapor path-delay calibration on the DSN antennas.[2] Although these measurements included few relatively strong radio sources, there were a sufficient number of weak sources for the purpose of evaluating the calibration technique. In this article, we report on an analysis of these measurements with respect to water-vapor radiometry and compare the results with water-vapor path-delay values obtained by a nearby dedicated WVR at Goldstone [15] and by stochastic estimation from Global Positioning System (GPS) receiver data at Goldstone. Since, for accurate measurements, the water-vapor path-delay retrieval algorithm may have seasonal and site dependence, we believe that the GPS measurements could serve as the absolute calibration of the water-vapor path delays for a given observing period and site, while the WVR formed by the antenna receiving system would measure short-time-scale fluctuations within the observing session.

II. Brightness-Temperature Measurements

The radiometric power measurement employed at the DSN sites is the conventional method of comparing the power received from a remote source with a calibrated local noise power; this method was first introduced by Dickey [21]. There were two sources of local noise power employed—a thermal radiator and a noise diode. In some of our measurements, only the thermal radiator was used as a power scale calibrator, while the others used both references.

The power at radio frequencies is usually described by an equivalent (brightness) temperature that is associated with blackbody radiation. At low frequencies, the blackbody radiation is well described by the Rayleigh–Jeans radiation law and, thus, the power can be uniquely described by the temperature of the radiation alone. At K-band frequencies, the deviation from the Rayleigh–Jeans law is not completely ignorable, and the first-order Planck radiation law correction yields that even a frequency-independent brightness temperature, T, becomes slightly frequency dependent if one insists upon using the brightness temperature defined by the Rayleigh–Jeans formula (ν is in GHz):

[2] This article, with minor changes, is a delayed publication of a manuscript from April 22, 1999.

$$T_{R-J} = T_{\text{Planck}} - \frac{1}{2}\left(\frac{h}{k}\right)\nu = T_{\text{Planck}} - 0.024\,\nu \tag{1}$$

The path of the radio signal from the main reflector of the antenna to the final values of digitized power include several stages of instrumentation. Therefore, the relationship between the real brightness temperature and the measured power is not necessary linear; however, an approximately linear relationship often is assumed. The common linear calibration of the brightness-temperature measurements consists of two reference radiators at temperatures T_a and T_b, and the power, P, measured by the receiving system can be expressed as

$$T = T_a + \frac{T_b - T_a}{P_b - P_a}(P - P_a) \tag{2}$$

In the the simplest linear calibration scheme, the DSN typically employs only one thermal radiator at T_b and uses the measured residual power value, P_a, at maximum attenuation that is associated with $T_a = 0$. The measurement of P_b usually is performed at the beginning and the end of each observing session for each frequency. Since this calibration method is not accurate enough, a noise diode also can be switched in on demand, and a linear calibration can be performed by setting T_b to the noise-diode temperature. The combination of these measurements also will allow a nonlinear calibration of the real brightness temperature as a function of measured power at a given frequency. The corresponding three-parameter quadratic calibration scheme is described in [22].

The temperature representing the measured power is decomposable into two components, the receiving-system temperature, T_r, and the sky temperature, T_{sky}:

$$T = T_r + T_{\text{sky}} \tag{3}$$

The brightness temperature, T_{sky}, includes the power of atmospheric radiation, point-like radio sources, and the cosmic background radiation. By this definition, the receiving-system temperature, T_r, includes all other sources of noise and, thus, it may be the function of time and, to a lesser degree, antenna pointing.

III. Brightness-Temperature to Water-Vapor Path-Delay Conversion

The phenomenon of propagation, emission, and absorption of electromagnetic radiation in the atmosphere is designated by Chandrasekhar as the process of "radiative transfer" [23]. The attenuation of external sources and the effective emission of atmospheric radiation are described by the radiative transfer equation expressed below in terms of brightness temperatures at microwave frequencies:

$$T_\nu = (T_s + T_c)\exp\big(-\tau_{\nu,\theta,\phi}(\infty)\big) + \int_0^\infty ds\, T_p(s)\frac{d\tau_{\nu,\theta,\phi}(s)}{ds}\exp\big(-\tau_{\nu,\theta,\phi}(s)\big) \tag{4}$$

where T_ν is the total brightness temperature of the sky at the given frequency, T_s is the brightness temperature of the radio source ($T_s = 0$ when no source is present), T_c is the cosmic background temperature, s is the path length of the radio signal measured from the receiver, T_p is the physical temperature of the atmosphere, and $\tau_{\nu,\theta,\phi}(s)$ is the opacity or optical depth of the atmosphere that is the path integral of the absorption coefficient $d\tau_{\nu,\theta,\phi}(s)/ds$. Besides the path length, the opacity also is a function of θ and ϕ, the elevation and azimuth angles, respectively. The primary components of the absorption coefficients include contributions from the 60-GHz oxygen spectrum band and the 22.35-GHz water-vapor spectral line. An additional component of opacity is due to condensed water [5].

With a given model of the opacity, Eq. (4), applied to a set of brightness-temperature measurements at different angular directions and oxygen-band frequencies, may be used to estimate the temperature profile, T_p, by an approximate numerical inversion of the obtained set of integral equations [24–26]. The water-vapor path-delay determination is an inverse form of the above process: assuming an a priori model of T_p, the integral equations of radiative transfer may be solved for the opacity and the related water-vapor density numerically or by a suitable analytic approximation. Applying a two-parameter water-vapor-density profile model, Robinson [27] argued the importance of the numerical solution of the unaltered radiative transfer equations as compared with the semiempirical analytic approximation of Resch [8,12]. However, his small improvement in the statistics of water-vapor path-delay retrieval does not sufficiently support this argument. The primary purpose of this article is a feasibility test of water-vapor radiometry with large DSN antennas and, therefore, only a cursory analysis of the water-vapor path-delay retrieval algorithm is within our concern at this time. For a clear understanding of the water-vapor path-delay retrieval process, we apply the simplest analytic approximation that coincides with the simplest retrieval formulation of [12]. This formulation by Resch [12] contains a single retrieval coefficient that can be transformed from the applied specific pair of frequencies to arbitrary frequencies based on the Lorentz shape of the spectral line. The description and justification of this retrieval algorithm is given in the Appendix.

IV. Results

Data retrieval and reduction involves two major steps: (1) total brightness-temperature determination and (2) water-vapor brightness temperature, opacity, and delay calculations. The total brightness temperatures were determined with the procedure outlined in Section II. Although additional noise diodes currently are being installed at all DSN sites, there were noise diodes only at the frequency-band centered $\nu_1 = 19.831$ in our experiments. Therefore, only the thermal radiator was used to calibrate the brightness temperature, resulting in an absolute calibration error as high as 5 percent, while the temporal drift of the calibration was approximately 2 percent. We expect to have better than 1 percent error for the absolute calibration and 0.3 percent for the drift with dual noise-diodes.

The radio-source temperatures were determined by pointing the antenna briefly off the source. The mean source temperature and its rms scatter were calculated for each observing session, and the strongest sources were removed from analysis. The elevation-angle-independent part of the measured effective water-vapor temperature at ν_1, $T_{A\,1\,w}$ (that includes the receiving-system temperature, T_r, which is dominated by the receiver electronic noise, T_e) and the mean zenith opacity were statistically estimated by Eq. (A-22), assuming a quadratic time dependence of $T_{A\,1\,w}$. The temperature $T_{A\,1\,w}$ drifted as much as 1 K during the course of an observation. For a particular observing session, the mean of the radio-source temperatures is absorbed by $T_{A\,1\,w}$ in the statistical fit using Eq. (A-22), but its scatter around the mean ($\approx$0.45 K) results in an error in water-vapor path delay. To reduce this effect, radio sources resulting in larger than 0.7-K residuals in the fit were removed. This limit was chosen as a compromise for retaining enough data and avoiding the removal of the non-Gaussian tail of water-vapor fluctuation [37]. This criterion was formulated as 0.7 K $>$ 10 $\times$ rms, where the rms of the final statistical fit was ranging between 0.03 and 0.08 K.

The water-vapor path delays were calculated from Eqs. (A-19) and (A-20) using the values of $T_{A\,1\,w}$ from the statistical fit. The obtained path-delay values were mapped to zenith by $\sin\theta$ and then compared with GPS and WVR estimates of zenith water-vapor path delays. The deviations between the DSS-14 estimates of zenith water-vapor path delays and the GPS/WVR estimates along with the mean opacities and source temperatures are given in Table 1 for each observing session at Goldstone in 1998.

The GPS path-delay estimates were made using GPS data from a GPS receiver 100 m from the antenna site. The dedicated WVR (J-series) is stationed at DSS 13. There are two measures of statistics for each observing session: (1) the mean of differences and (2) the root-mean-square of the differences.

Table 1. Summary of experiments.

Date	DOY	Duration, UT	Mean zenith opacity τ_{Zw}	Source temperature, K		Difference, cm			
						DSS 14 − GPS		DSS 14 − WVR	
				Mean	rms	Mean	rms	Mean	rms
10-08	281	20:00–05:00	0.013	0.29	0.4	0.30	0.39	0.87	0.95
10-24	297	20:00–05:00	0.043	0.51	0.5	−0.34	0.79	0.74	0.94
10-28	301	12:30–18:00	0.029	0.58	0.4	0.18	0.41	0.10	0.28

For our water-vapor delay errors, these differences are dominated by the source temperature fluctuation (≈0.35 cm), the brightness-temperature calibration error (5 percent or <0.5 cm), and the scale error of the path-delay retrieval algorithm (<5 percent or ≤0.5 cm).

The effective water-vapor brightness temperature as a function of air mass and the zenith path delay as a function of time are shown in Figs. 1 through 3. These figures also include the stochastically estimated zenith delays from GPS measurements and the dedicated WVR estimates of zenith delays. The WVR was pointing to zenith.

Two of the GPS path delays were extracted from the routine site-specific FLINN solution. The path delays in Fig. 1 were determined by Y. Bar-Sever in a nonroutine fashion, but this is still a nonoptimal method, since the 24-hour solutions produce gaps at the day boundaries.

The WVR, stationed at DSS 13, is separated from DSS 14 by approximately 20 km. The 20-km distance between DSS 14 and the dedicated WVR may explain some of the discrepancies between the path delays determined by the dedicated WVR and the other methods, although the deviation from the GPS values in Fig. 1, nearly as high as 1 cm, is somewhat puzzling at the 2-cm path-delay level.

In summary, the measurements presented in this article were not ideal for precision water-vapor radiometry because of the presence of radio sources and an incomplete precision brightness-temperature calibration system. Nevertheless, we have developed the data path from the receiving system with a set of computerized analytical tools to process the data, and the first results appear to be quite reasonable.

V. Conclusion

The exploratory brightness-temperature measurements combined with the presented water-vapor path-delay retrieval algorithm indicate that the DSN antennas may be utilized as dual-frequency water-vapor radiometers. The lowest system temperature scatter is 0.034 K; that is an indicator of the lowest achievable error of this technique (0.03-cm path delay at zenith). The root-mean-square difference between the obtained delay values and the stochastically estimated values from the GPS receiver data varies between 0.3 and 0.8 cm at zenith, while the mean difference is below 0.4 cm. The known sources of these differences include unwanted source-temperature variations and an inadequate brightness-temperature calibration. Due to the exploratory nature of this study, the water-vapor path-delay retrieval algorithm was not fully explored; the simplest method was used and, thus, there is room for improvements. For a validation of the technique, we plan to perform more measurements without radio sources at each DSN site with two-frequency systematic calibration of the brightness temperature and to adjust the retrieval algorithm if necessary. We think that the GPS delay values could be used for normalization of the retrieval algorithm and that the comparison between the delay values given by the WVR formed by the DSN antennas and the GPS estimates potentially may help to improve the GPS estimation technique.

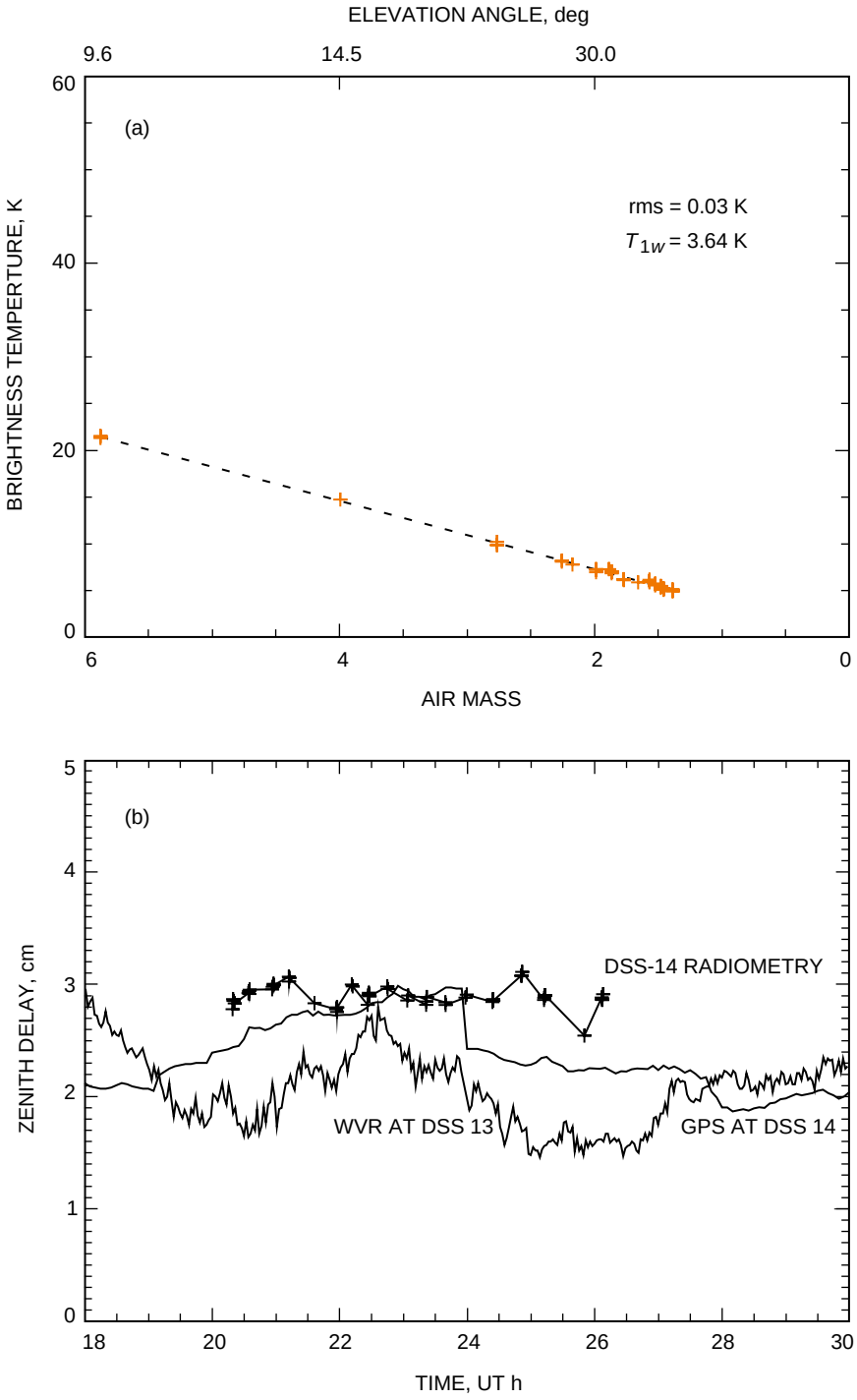

Fig. 1. Measurements taken at DSS 14 at Goldstone, California, on October 8, 1998 (DOY 281): (a) effective brightness temperature and (b) zenith path delay of water vapor. The "+" symbols represent the radiometry at DSS 14; the solid line is the GPS estimates at DSS 14; and the rapidly fluctuating points are the zenith path-delay measurements by the WVR at DSS 13.

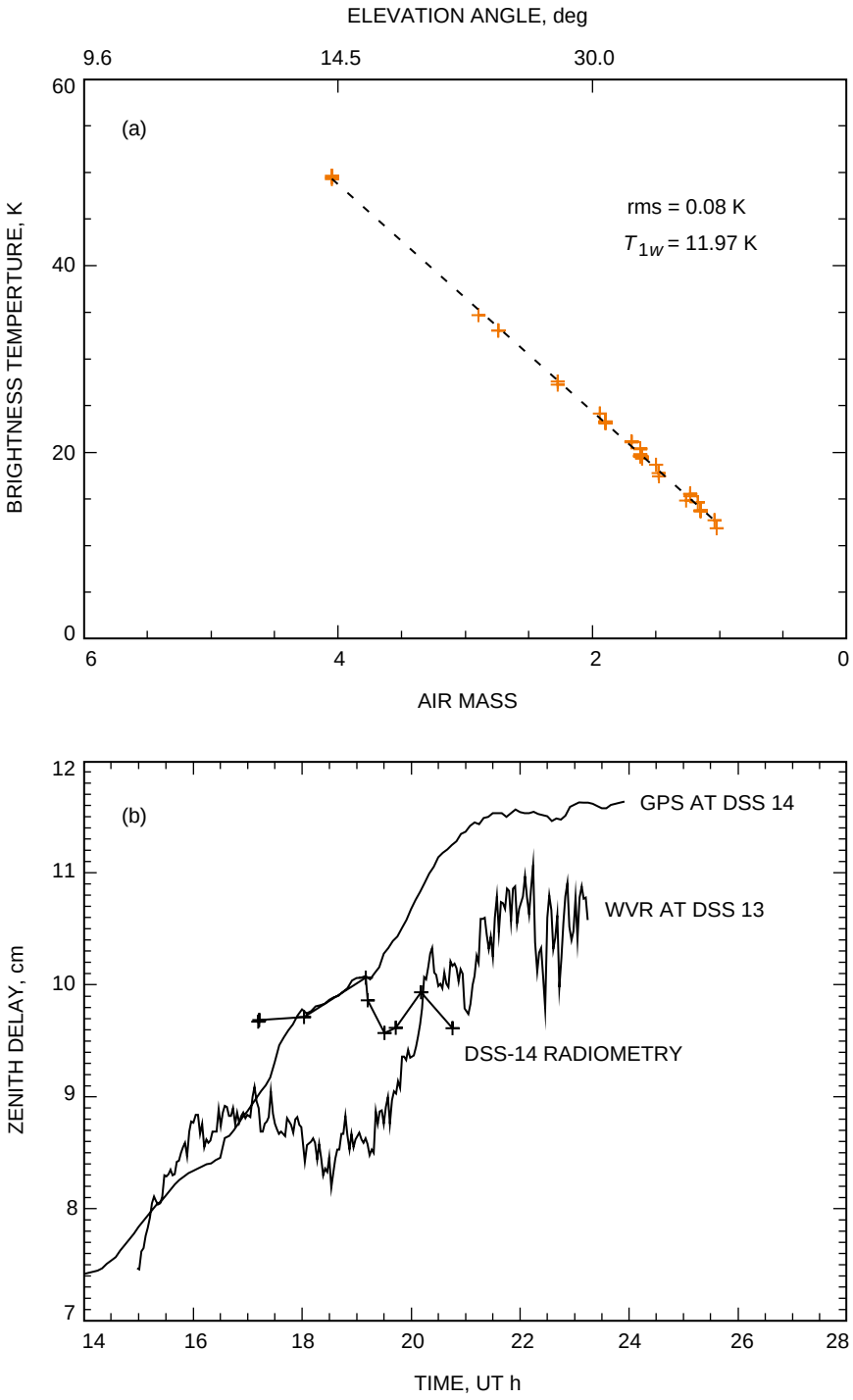

Fig. 2. Measurements taken at DSS 14 at Goldstone, California, on October 24, 1998 (DOY 297): (a) effective brightness temperature and (b) zenith path delay of water vapor. The "+" symbols represent the radiometry at DSS 14; the solid line is the GPS estimates at DSS 14; and the rapidly fluctuating points are the zenith path-delay measurements by the WVR at DSS 13.

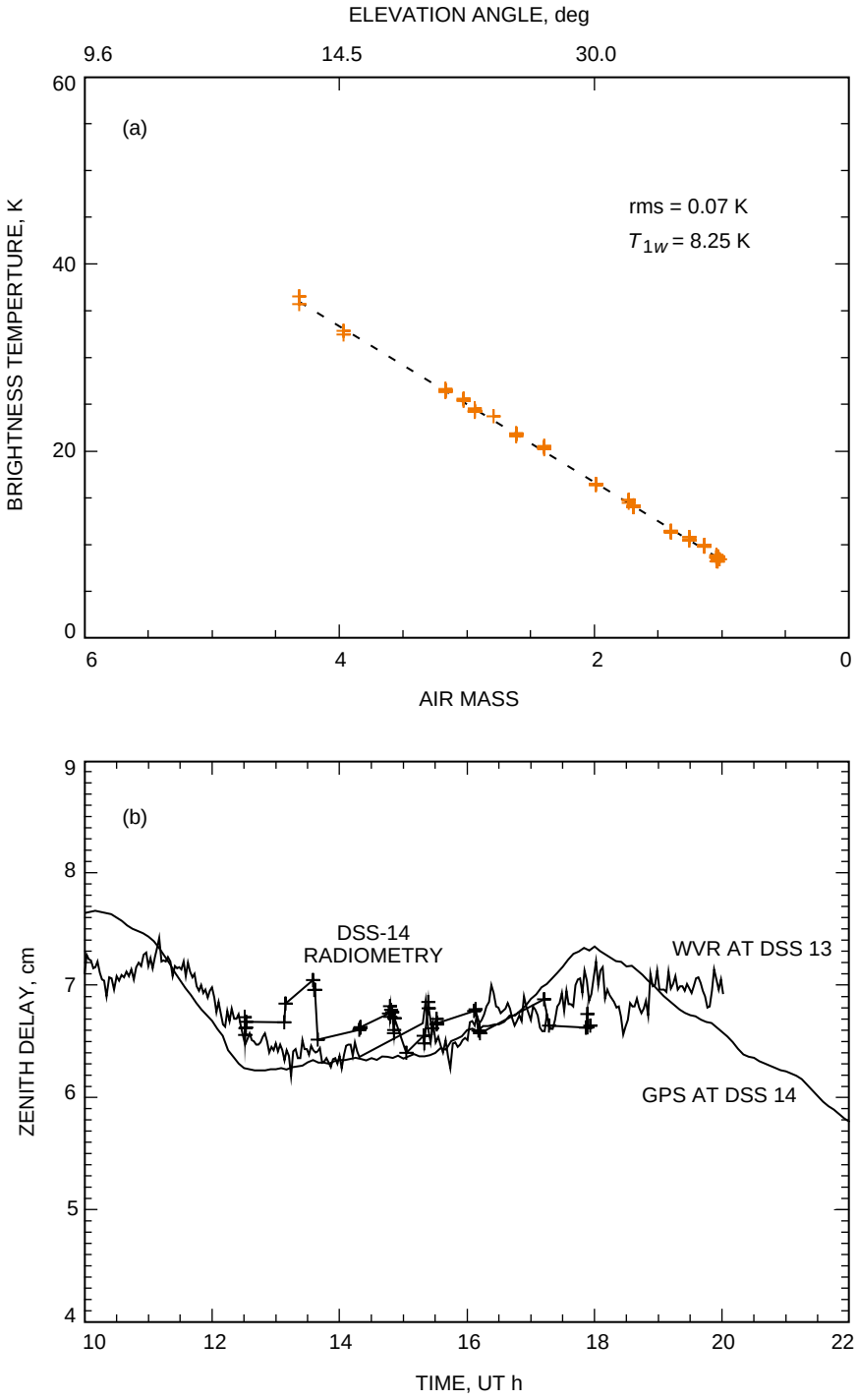

Fig. 3. Measurements taken at DSS 14 at Goldstone, California, on October 28, 1998 (DOY 301): (a) effective brightness temperature and (b) zenith path delay of water vapor. The "+" symbols represent the radiometry at DSS 14; the solid line is the GPS estimates at DSS 14; and the rapidly fluctuating points are the zenith path-delay measurements by the WVR at DSS 13.

Acknowledgments

The GPS water-vapor delay values were kindly provided by Y. Bar-Sever and D. Jefferson from the FLINN GPS database. We also appreciate the help of S. Keihm in supplying us with the WVR delay values extracted from the WVR that is operated continuously at the Goldstone DSS-13 site. We also acknowledge review of the manuscript by G. Resch; his comments are well appreciated.

References

[1] T. A. Herring, J. L. Davis, and I. I. Shapiro, "Geodesy by Radiointerferometry: The Application of Kalman Filtering to the Analysis of VLBI Data," *J. Geophys. Res.*, vol. 95, pp. 12,561–12,581, 1990.

[2] R. N. Treuhaft and G. E. Lanyi, "The Effect of Dynamic Wet Troposphere on Radio Interferometric Measurements," *Radio Science*, vol. 22, pp. 251–265, 1987.

[3] S. M. Lichten, "Estimation and Filtering Techniques for High-Accuracy GPS Applications," *The Telecommunications and Data Acquisition Progress Report 42-97, January–March 1989*, Jet Propulsion Laboratory, Pasadena, California, pp. 1–20, May 15, 1989.
http://tmo.jpl.nasa.gov/tmo/progress_report/42-97/97A.PDF

[4] S. M. Lichten, "Precise Estimation of Tropospheric Path Delays With GPS Techniques," *The Telecommunications and Data Acquisition Progress Report 42-100, October-December 1989*, Jet Propulsion Laboratory, Pasadena, California, pp. 1–12, February 15, 1990.
http://tmo.jpl.nasa.gov/tmo/progress_report/42-100/100A.PDF

[5] D. H. Staelin, "Measurements and Interpretation of the Microwave Spectrum of the Terrestrial Atmosphere Near 1-cm Wavelength," *J. Geophys. Res.*, vol. 71, pp. 2875–2882, 1966.

[6] E. R. Westwater, "The Accuracy of Water Vapor and Cloud Liquid Determination by Dual-Frequency Ground Based Microwave Radiometry," *Radio Science*, vol. 13, pp. 677–685, 1978.

[7] E. R. Westwater, "Ground Based Microwave Radiometric Retrieval of Precipitable Water Vapor in the Presence of Clouds With High Liquid Content," *Radio Science*, vol. 15, pp. 947–957, 1980.

[8] E. S. Claflin, S. C. Wu, and G. M. Resch, "Microwave Radiometer Measurement of Water Vapor Path Delay: Data Reduction Techniques," *The Deep Space Network Progress Report 42-48, September and October 1978*, Jet Propulsion Laboratory, Pasadena, California, pp. 22–30, October 15, 1978.

[9] S. C. Wu, "Optimum Frequencies of a Passive Microwave Radiometer for Tropospheric Path-Length Correction," *IEEE Transactions on Geoscience and Remote Sensing*, vol. AP-27, no. 2, pp. 233–239, 1979.

[10] G. M. Resch, "Water Vapor: The Wet Blanket of Microwave Interferometry," in *Atmospheric Water Vapor*, edited by A. Deepak, T. D. Wilkerson, and L. H. Ruhnke, New York: Academic Press, pp. 205–282, 1980.

[11] G. M. Resch, M. C. Chavez, and N. I. Yamane, "Description and Overview of an Instrument Designed to Measure Line-of-Sight Delay Due to Water Vapor," *The Telecommunications and Data Acquisition Progress Report 42-72, October–December 1982*, Jet Propulsion Laboratory, Pasadena, California, pp. 1–19, February 15, 1983.
http://tmo.jpl.nasa.gov/tmo/progress_report/42-72/72A.PDF

[12] G. M. Resch, "Inversion Algorithms for Water Vapor Radiometers Operating at 20.7 and 31.4 GHz," *The Telecommunications and Data Acquisition Progress Report 42-76, October–December 1983*, Jet Propulsion Laboratory, Pasadena, California, pp. 12–26, February 15, 1984.
http://tmo.jpl.nasa.gov/tmo/progress_report/42-76/76B.PDF

[13] G. M. Resch, "Another Look at the Optimum Frequencies for a Water Vapor Radiometer," *The Telecommunications and Data Acquisition Progress Report 42-76, October–December 1983*, Jet Propulsion Laboratory, Pasadena, California, pp. 1–11, February 15, 1984.
http://tmo.jpl.nasa.gov/tmo/progress_report/42-76/76A.PDF

[14] M. A. Jansen, "A New Instrument for the Determination of Radio Path Delay Due to Atmospheric Water Vapor," *IEEE Transactions on Geoscience and Remote Sensing,* vol. GE-23, no. 5, pp. 485–490, 1985.

[15] S. J. Keihm, "Water Vapor Radiometer Measurements of the Tropospheric Delay Fluctuations at Goldstone Over a Full Year," *The Telecommunications and Data Acquisition Progress Report 42-122, April–June 1995*, Jet Propulsion Laboratory, Pasadena, California, pp. 1–11, August 15, 1995.
http://tmo.jpl.nasa.gov/tmo/progress_report/42-122/122J.pdf

[16] S. J. Keihm, "Advanced Algorithm and System Development for Cassini Radio Science Tropospheric Calibration," *The Telecommunications and Data Acquisition Progress Report 42-127, July–September 1996*, Jet Propulsion Laboratory, Pasadena, California, pp. 1–19, November 15, 1996.
http://tmo.jpl.nasa.gov/tmo/progress_report/42-127/127A.pdf

[17] R. P. Linfield and J. Z. Wilcox, "Radio Metric Errors Due to Mismatch and Offset Between a DSN Antenna Beam and the Beam of a Troposphere Calibration Instrument," *The Telecommunications and Data Acquisition Progress Report 42-114, April–June 1993*, Jet Propulsion Laboratory, Pasadena, California, pp. 1–13, August 15, 1993.
http://tmo.jpl.nasa.gov/tmo/progress_report/42-114/114A.pdf

[18] R. Linfield, "The Effect of Aperture Averaging Upon Tropospheric Delay Fluctuations Seen With a DSN Antenna," *The Telecommunications and Data Acquisition Progress Report 42-124, October–December 1995*, Jet Propulsion Laboratory, Pasadena, California, pp. 1–7, February 15, 1996.
http://tmo.jpl.nasa.gov/tmo/progress_report/42-124/124A.pdf

[19] C. T. Stelzried, L. Skjerve, and G. Bury, "DSS-13 26-Meter Antenna Upgraded Radiometer System," *The Telecommunications and Data Acquisition Progress Report 42-109, January–March 1992*, Jet Propulsion Laboratory, Pasadena, California, pp. 209–220, May 15, 1992.
http://tmo.jpl.nasa.gov/tmo/progress_report/42-109/109Q.PDF

[20] M. S. Gatti, S. R. Stewart, J. G. Bowen, and E. B. Paulsen, "A Radio Telescope for the Calibration of Radio Sources at 32 Gigahertz," *The Telecommunications and Data Acquisition Progress Report 42-118, April–June 1994*, Jet Propulsion Laboratory, Pasadena, California, pp. 56–82, August 15, 1994.
http://tmo.jpl.nasa.gov/tmo/progress_report/42-118/118G.pdf

[21] R. H. Dickey, R. Beringer, R. L. Kyhl, and A. B. Vane "Atmospheric Absorption Measurements with a Microwave Radiometer," *Phys. Rev.*, vol. 70, pp. 340–348, 1946.

[22] C. T. Stelzried and M. J. Klein, "Precision DSN Radiometric Systems: Impact on Microwave Calibrations," *Proc. of the IEEE*, vol. 82, pp. 776–787, May 1994.

[23] S. Chandrasekhar, *Radiative Transfer*, New York: Dover Publications, 1960.

[24] M. T. Chahine, "Inverse Problems in Radiative Transfer: Determination of Atmospheric Parameters," *Journal of the Atmospheric Sciences*, vol. 27, no. 6, pp. 960–967, 1970.

[25] E. R. Westwater, "Ground-Based Determination of Low Altitude Temperature Profiles by Microwaves," *Monthly Weather Review*, vol. 100, no. 1, pp. 15–28, 1972.

[26] J. B. Snider, "Ground-Based Sensing of Temperature Profiles from Angular and Multi-Spectral Microwave Emission Measurements," *J. of Appl. Meteorology*, vol. 11, no. 6, pp. 958–967, 1972.

[27] S. E. Robinson, "A New Algorithm for Microwave Delay Estimation From Water Vapor Radiometer Data," *The Telecommunications and Data Acquisition Progress Report 42-87, July–September 1986*, Jet Propulsion Laboratory, Pasadena, California, pp. 149–157, November 15, 1986.
http://tmo.jpl.nasa.gov/tmo/progress_report/42-87/87P.PDF

[28] G. Lanyi, "Tropospheric Delay Effects in Radio Interferometry," *The Telecommunications and Data Acquisition Progress Report 42-78, April–June 1984*, Jet Propulsion Laboratory, Pasadena, California, pp. 152–159, August 15, 1984.
http://tmo.jpl.nasa.gov/tmo/progress_report/42-78/78N.PDF

[29] J. H. Van Vleck and V. F. Weisskopf, "On the Shape of Collision-Broadened Lines," *Rev. Mod. Phys*, vol. 17, p. 227, 1945.

[30] D. D. Morabito and L. Skjerve, "Analysis of Tipping-Curve Measurements Performed at the DSS-13 Beam-Waveguide Antenna at 32 and 8.45 Gigahertz," *The Telecommunications and Data Acquisition Progress Report 42-122, April–June 1995*, Jet Propulsion Laboratory, Pasadena, California, pp. 151–174, August 15, 1995.
http://tmo.jpl.nasa.gov/tmo/progress_report/42-122/122C.pdf

[31] D. Morabito, R. Clauss, and M. Speranza, "Ka-Band Atmospheric Noise-Temperature Measurements at Goldstone, California, Using a 34-Meter Beam-Waveguide Antenna," *The Telecommunications and Data Acquisition Progress Report 42-132, October–December 1997*, Jet Propulsion Laboratory, Pasadena, California, pp. 1–20, February 15, 1998.
http://tmo.jpl.nasa.gov/tmo/progress_report/42-132/132B.pdf

[32] J. Saastamoinen, "Atmospheric Correction for the Troposphere and Stratosphere in Radio Ranging Satellites," in *The Use of Artificial Satellites for Geodesy*, Geophysical Monograph 15, American Geophysical Union, Washington, D.C., pp. 247–251, 1972.

[33] J. W. Waters, "Absorption and Emission by Atmospheric Gases," *Methods of Experimental Physics: Astrophys.*, edited by M. L. Meeks, part B, vol. 12, New York: Academic Press, pp. 142–175, 1976.

[34] C. S. Gardner, "Correction of Laser Tracking Data for the Effects of Horizontal Refractivity Gradients," *Appl. Opt.*, vol. 16, pp. 2427–2433, 1977.

[35] G. Chen and T. A. Herring, "Effects of Atmospheric Azimuthal Asymmetry on the Analysis of Space Geodetic Data," *J. of Geophys. Res.*, vol. 102, no. B9, pp. 20,489–20,502, 1997.

[36] E. K. Smith and S. Weintraub, "The Constants in the Equation for Atmospheric Refractive Index at Radio Frequencies," *Proc. IRE*, vol. 41, pp. 1035–1057, 1953.

[37] C. J. Naudet, "Estimation of Tropospheric Fluctuations Using GPS Data," *The Telecommunications and Data Acquisition Progress Report 42-126, April–June 1996*, Jet Propulsion Laboratory, Pasadena, California, pp. 1–19, August 15, 1996.
http://tmo.jpl.nasa.gov/tmo/progress_report/42-126/126A.pdf

[38] A. B. Tanner, "Development of a High-Stability Water Vapor Radiometer," *Radio Science*, vol. 33, pp. 449–462, 1998.

Appendix

Water-Vapor Path-Delay Retrieval Algorithm

Equation (4) is analytically integrable for a constant T_p, and the mean value theorem of integrals, after a change of variables, produces a formally equivalent result for an arbitrary vertical temperature profile:

$$T = (T_s + T_c)\exp\big(-\tau_{\nu,\theta,\phi}(\infty)\big) + T_p(\langle h\rangle)\big(1-\exp\big(-\tau_{\nu,\theta,\phi}(\infty)\big)\big) \tag{A-1}$$

In Eq. (A-1), T_p is assumed to be laterally homogeneous. The quantity $\langle h\rangle$ is a priori unknown and, in principle, it could be a complicated functional of the opacity. However, T_p varies only about 10 percent up to about an altitude of 4 km, the region that includes more than 80 percent of the total water vapor. Therefore, T_p cannot depend strongly on $\langle h\rangle$ when Eq. (A-1) refers to the opacity of water vapor only and, thus, T_p is only a weak function of the water-vapor opacity. In general, the opacity is a sum of the oxygen, water vapor, and condensed water terms; the opacity of the oxygen is relatively low—less than 0.02 at 20 GHz and zenith. The opacity of the water vapor can be in the order of unity for high water-vapor content and low-elevation angles, but it stays <0.25 at moderately dry climates and $\theta > 10$ deg.

Consequently, for the moderately dry DSN climates, the exponential function in the integral of Eq. (4) may be linearized with an estimated error of <5 percent. Note that the water-vapor component of the absorption coefficient $d\tau_{\nu,\theta,\phi}(s)/ds$ is proportional to the water-vapor density and, therefore, for a linear temperature profile, one can show the equivalence of $\langle h\rangle$ to the mean height of the water-vapor distribution. With these assumptions, for an exponential model of the water-vapor distribution, $\langle h\rangle$ is then the scale height, Δ_w, of the distribution. Considering that, on the average, the temperature profile may be characterized by a mean surface temperature, $\langle T_p(0)\rangle$, and the mean tropospheric lapse rate, $\langle w\rangle$, the physical temperature term in Eq. (A-1) may be approximated as

$$T_p(\langle h \rangle) = \langle T_p(0) \rangle - \langle w \rangle \langle h \rangle \tag{A-2}$$

At the mid-latitude climate of the DSN sites, $\langle T_p(0) \rangle = 292$ K and $\langle w \rangle = 6.82$ K/km, while $\langle h \rangle = 2.2$ km for a mean exponential model of the water-vapor distribution [28], resulting in a mean value for $T_p(\langle h \rangle)$ of 277 K. This value can be adjusted to individual days, keeping in mind the fact that the surface temperature in Eq. (A-2) is considered as an average of measured values over at least the day. It also should be noted that, under certain seasons and climates, the lower 2-km portion of the atmosphere cannot always be characterized by the upper tropospheric lapse rate and, thus, Eq. (A-2) does not apply. At high water-vapor content and low-elevation angles, Eq. (A-1) certainly needs some correction if $\langle h \rangle$ is identified with the scale height of water vapor.

In the frequency region of from 10 to 30 GHz, the absorption coefficient of the oxygen, and the condensed water as well [5], is proportional to ν^2. Staelin [5] proposed removing the condensed-water term by forming the quadratic-frequency-term free quantity $\tau_1 - (\nu_1/\nu_2)^2 \tau_2$; the opacities are obtained from dual-frequency measurements at ν_1 and ν_2 ($\tau_1 = \tau_{\nu_1,\theta,\phi}$ and $\tau_2 = \tau_{\nu_2,\theta,\phi}$). The opacity of the oxygen can be calculated from the emission model of the oxygen; the result of such a calculation was applied in [30,31] to single-frequency (32-Ghz) antenna temperature measurements on a DSN 32-m antenna. In this article, we adopt the scheme of Staelin for the removal of the opacity of oxygen; in an extension of this work, we plan to incorporate the oxygen-opacity calculation for determining the condensed-water contribution as an additional check. After a suitable normalization, the quadratic-frequency-term free quantity represents the opacity of the water vapor at a given frequency; we adopt the lower frequency, ν_1, as the reference:

$$\tau_{1\,w} = N_1 \left(\tau_1 - \left(\frac{\nu_1}{\nu_2} \right)^2 \tau_2 \right) \tag{A-3}$$

The frequency dependence of the absorption coefficient is nearly Lorentzian [29] and, therefore, the opacity has the same behavior. At a given frequency, the opacity is the sum of water vapor, condensed (liquid) water, and oxygen:

$$\tau_\nu = \tau_{\nu\,w} + \tau_{\nu\,l} + \tau_{\nu\,o} \tag{A-4}$$

However, due to the quadratic frequency dependence of the last two terms, one may replace τ_1 and τ_2 by $\tau_{1\,w}$ and $\tau_{2\,w}$, respectively. Thus, the normalization factor N_1 can be obtained by substituting the Lorentzian functional form of the opacity of water vapor,

$$\tau_{\nu,\theta,\phi} = \frac{m(\theta,\phi)\tau_{0\,Z}}{1 + \dfrac{(\nu - \nu_0)^2}{\sigma^2}} \tag{A-5}$$

into Eq. (A-3). Here, ν_0 is the center frequency of the water-vapor line, $\nu_0 = 22.235$ GHz; σ is the thermodynamically widened line width, $\sigma \approx 3$ GHz [33]; $\tau_{0\,Z}$ is the opacity at ν_0 and zenith; and $m(\theta,\phi)$ is the linear air-mass mapping function from zenith to the line of sight. In the flat-Earth approximation, the average $m(\theta,\phi)$ equals $1/\sin\theta$ if the azimuthal asymmetry of the mean opacity is ignored. For high water-vapor content and low-elevation angles, corrections to $1/\sin\theta$ should be considered [28,32,34,35]. The obtained normalization factor is

$$N_1 = \frac{1}{1 - \left(\dfrac{\nu_1}{\nu_2} \right)^2 \dfrac{\tau_{\nu_2,\theta,\phi}}{\tau_{\nu_1,\theta,\phi}}} = \frac{1}{1 - \left(\dfrac{\nu_1}{\nu_2} \right)^2 R_L(\nu_2,\nu_1)} \tag{A-6}$$

where $R_L(\nu_2, \nu_1)$ is the Lorentzian ratio

$$R_L(\nu_2, \nu_1) = \frac{\tau_{\nu_2,\theta,\phi}}{\tau_{\nu_1,\theta,\phi}} = \frac{1 + \dfrac{(\nu_1 - \nu_0)^2}{\sigma^2}}{1 + \dfrac{(\nu_2 - \nu_0)^2}{\sigma^2}} \tag{A-7}$$

For the measurements presented in this article, $\nu_1 = 19.831$ GHz and $\nu_2 = 26.231$ GHz; these numbers result in $R_L(\nu_2, \nu_1) = 0.57$ and $N_1 = 1.48$. The water-vapor path delay then is calculated from the dominant (polar) term of the refractivity of the water vapor [36]:

$$\Delta s = K \int_0^\infty ds \, \frac{\rho_w(s)}{T_p(s)} \tag{A-8}$$

where ρ_w is the water-vapor density. Equation (A-8) may be evaluated, after substitution, by the mean value theorem of integrals with the same assumptions used in the opacity integral:

$$\Delta s = \frac{K}{T_p(\langle h \rangle)} \int_0^\infty ds \, \rho_w(s) \tag{A-9}$$

Since the opacity of the water vapor is proportional to the path integral of the water-vapor density, a linear relationship between Δs and $\tau_{1\,w}$ is obtained:

$$\Delta s = A_1 \tau_{1\,w} = A_1 N_1 \left(\tau_1 - \left(\frac{\nu_1}{\nu_2} \right)^2 \tau_2 \right) \tag{A-10}$$

Based on theoretical calculations and actual measurements of the emission spectra and refractivity of the water vapor, one can determine the water-vapor retrieval coefficient, A_1, in Eq. (A-10). In this article, we adapt and modify the mean value obtained in [12] by Resch for the JPL water-vapor radiometers. This process will illustrate that certain retrieval algorithms of a particular WVR may be applied to another one with modification. A biasless linear expression in opacities is given in [12] and can be written as

$$\Delta s = 158 \left(\tau_1' - \left(\frac{\nu_1'}{\nu_2'} \right)^2 \tau_2' \right) \tag{A-11}$$

where Δs is in centimeters, and $\nu_1' = 20.7$ GHz and $\nu_2' = 31.4$ GHz. First, we transform Eq. (A-11) so that it refers to the water-vapor opacity at ν_1': $\Delta s = (158/N_1')\tau_{1\,w}' = 149.6\tau_{1\,w}'$. Since the water-vapor path delay is independent of the retrieval frequencies, we can transform Eq. (A-11) to the frequency ν_1:

$$\Delta s = \left(\frac{149.6\tau_{1\,w}'}{\tau_{1\,w}} \right) \tau_{1\,w} = A_1 N_1 \left(\tau_1 - \left(\frac{\nu_1}{\nu_2} \right)^2 \tau_2 \right) \tag{A-12}$$

where

$$A_1 = 149.6 R_L(\nu_1, \nu_1') \tag{A-13}$$

The actual frequencies used for our measurements lead to $R_L(\nu_1, \nu_1') = 0.76$ and $A_1 = 114.4$ cm. For low opacity values in Eq. (A-1), only the first-order opacity term may be retained, giving a linear relationship between the brightness temperature of the sky and the opacity:

$$T_\nu = T_s + T_c + \big(T_p(\langle h \rangle) - T_s - T_c\big)\tau_{\nu,\theta,\phi}(\infty) \tag{A-14}$$

Actual measurements of brightness temperatures involve the sum of the sky and the receiving-system temperatures. If the receiving-system temperature, T_r, is not calibrated, then we must include it in our brightness-temperature equation used for data reduction. If T_r is calibrated, then we still include it as a representation of calibration error. Adding T_r to Eq. (A-14) and collecting all temperatures into two linear coefficients, Eq. (A-14) can be written for the total measured temperature (operating temperature) as

$$T_\nu = T_{A\,\nu} + T_B\,\tau_{\nu,\theta,\phi}(\infty) \tag{A-15}$$

$$T_{A\,\nu} = T_s + T_c + T_r \tag{A-16}$$

$$T_B = T_p(\langle h \rangle) - T_s - T_c \tag{A-17}$$

Defining the effective brightness temperature of water vapor as

$$T_{\nu\,w} = T_B\,\tau_{\nu\,w} \tag{A-18}$$

then the combination of Eqs. (A-3) and (A-18) yields the effective water-vapor brightness temperature and path delay:

$$T_{1\,w} = N_1 \left(T_1 - \left(\frac{\nu_1}{\nu_2}\right)^2 T_2 \right) - T_{A\,1\,w} \tag{A-19}$$

$$\Delta s = \frac{A_1 T_{1\,w}}{T_B} \tag{A-20}$$

where

$$T_{A\,1\,w} = N_1 \left(T_{A\,1} - \left(\frac{\nu_1}{\nu_2}\right)^2 T_{A\,2} \right) \tag{A-21}$$

In T_B, the frequency dependence of T_s and T_c is ignored. In the data reduction of brightness-temperature measurements, T_A is statistically estimated for the entire observing session as a quadratic function of time. Assuming azimuthal symmetry and ignoring the curvature of the Earth, the statistical fit determines $T_{A\,1\,w}$ and the average zenith opacity, $\tau_{Z\,w}$, from Eqs. (A-3) and (A-15):

$$T_{A\,1\,w} + \frac{\tau_{1\,Z\,w} T_B}{\sin\theta} = N_1 \left(T_1 - \left(\frac{\nu_1}{\nu_2}\right)^2 T_2 \right) \tag{A-22}$$